




Optimisation of microwave absorption properties of Fe-substituted $Y_2Co_{17-x}Fe_x$ soft-magnetic composites

Jinpeng Zhong^{1,2,3}, Guoguo Tan^{1,2,*} , Qikui Man^{1,2}, Mingqiang Ning^{1,2}, Yu Gao^{1,2}, Xincai Liu^{3,*}, and Jing Pan³

¹Key Laboratory of Magnetic Materials and Devices, Ningbo Institute of Materials Technology & Engineering, Chinese Academy of Sciences, Ningbo 315201, Zhejiang, China

²Zhejiang Province Key Laboratory of Magnetic Materials and Application Technology, Ningbo Institute of Materials Technology & Engineering, Chinese Academy of Sciences, Ningbo 315201, Zhejiang, China

³Faculty of Materials Science and Chemical Engineering, Ningbo University, Ningbo 315211, China

Received: 30 April 2021

Accepted: 3 October 2021

Published online:
11 October 2021

© The Author(s), under exclusive licence to Springer Science+Business Media, LLC, part of Springer Nature 2021

ABSTRACT

The increase in electromagnetic wave pollution at high frequency (gigahertz band) has led to an increasing demand for more effective microwave absorption materials (MAMs). This study aims to investigate magneto-crystalline anisotropy materials as MAMs. Magnetic and microwave absorption properties of $Y_2Co_{17-x}Fe_x$ ($x = 0, 5, 9, 13, 17$) are reported in this study. As the Fe content increases, the magneto-crystalline anisotropy of $Y_2Co_{17-x}Fe_x$ changes from planar anisotropy to axis, then to cone, and eventually to plane. Meanwhile, the variation trend of the magnetization (M_s) value increases first and then decreases, reaching a maximum at $x = 9$. The $Y_2Co_{17-x}Fe_x$ /paraffin composites ($x = 0, 13, 17$) with the planar anisotropy show stronger reflection loss (RL) than that composite ($x = 5$) with the uniaxial anisotropy. The strongest RL value is achieved for the conical anisotropy composites ($x = 9$). This composite, with conical anisotropy and highest M_s , exhibits the highest gigahertz frequency permeability, which is advantageous for improving the impedance matching and attenuation abilities of microwave absorption. The $Y_2Co_8Fe_9$ /paraffin composite exhibits a reflection loss value of -46.9 dB and effective absorption bandwidth (EAB, $RL < -10$ dB) of 4.74 GHz with a thickness of 2.0 mm at 10.2 GHz, suggesting its applicability as an efficient microwave absorbent in the gigahertz frequency.

Address correspondence to E-mail: kant01@126.com; liuxincai@nbu.edu.cn

1 Introduction

The development of communication technologies has led to a rapid increase in effective, multifunctional, and intelligent devices, such as mobile phones, smart wearable devices, and autonomous cars. To reduce the size and to improve the performance of such devices, the operating frequencies of various electronic devices have become increasingly higher. There is a significant trend in the increasing application of gigahertz (GHz) frequency devices. As a result, electromagnetic wave pollution under high-frequency (GHz band) conditions has become a serious problem, because it not only interferes with the normal operation of electronic devices but also is potentially detrimental to human health [1–4]. Therefore, to mitigate this pollution and its hazardous effects, use of effective MAMs is desired. Traditional soft-magnetic materials such as metallic magnetic materials [5, 6] and ferrites [7, 8] have been extensively researched as candidate MAMs because they exhibit both magnetic loss and electric loss properties [9, 10]. However, the permeability of spinel ferrites and metallic materials decreases rapidly with increasing frequency, as expressed by the Snoek limit [11]:

$$f_r(\mu_i - 1) = \frac{1}{3\pi} \gamma M_s \quad (1)$$

where f_r , μ_i , γ , and M_s are the resonance frequency, initial permeability, gyromagnetic ratio, and saturation magnetisation, respectively. The right side of Eq. 1 is constant because saturation magnetisation (M_s) and gyromagnetic ratio (γ) are fixed for a given magnetic material. This suggests that initial permeability (μ_i) and natural resonance frequency (f_r) are competing factors, suggesting that a high permeability value cannot be obtained at high frequencies. In order to obtain high GHz range absorption performance, the soft-magnetic materials should exhibit high permeability and high resonance frequency [12–14]. This illustrates how a given material is limited in terms of effective electromagnetic absorption.

For magnetic materials with planar anisotropy, the Snoek limit can be modified as [15]:

$$f_r(\mu_i - 1) = \frac{1}{4\pi} \gamma M_s \sqrt{\frac{H_0}{H_\phi}} \quad (2)$$

where H_0 and H_ϕ are the out-of-plane anisotropy field and in-plane anisotropy field, respectively. For a

planar anisotropy material, H_0 is much larger than H_ϕ [16]. This suggests that the value on the right side of Eq. 2 could be much higher than that of Eq. 1. This means that the Snoek limit can be augmented using the planar anisotropy modification, whereby high permeability and high resonance frequency can be obtained simultaneously. On the basis of this theory, many efforts have been devoted to finding a planar anisotropy material with high soft-magnetic properties at higher frequencies [17]. Hexagonal ferrites, such as Co_2Z -type ferrites, have intrinsic magneto-crystalline anisotropy and can be used in high-frequency applications [18, 19]. However, ferrites with low M_s cannot satisfy the requirement for further optimisation of their high-frequency properties.

Compared to Co_2Z -type ferrites, rare-earth intermetallic compounds have attracted widespread attention because of their higher saturation magnetisation and resonance frequency. A series of planar anisotropy $\text{R}_2\text{Fe}_{17}\text{N}_{3-8}$ [15, 20], $\text{R}_2\text{Fe}_{14}\text{B}$ [21, 22], and R_2Co_{17} [23, 24] (R = rare-earth element) compounds with high permeability and resonance frequency were prepared and their high microwave absorbing properties have also been reported. However, a small amount of $\alpha\text{-Fe}$ is an undesirable by-product in the process of nitriding for $\text{R}_2\text{Fe}_{17}\text{N}_{3-8}$. Complex preparation is also not suitable for mass production application. Meanwhile, the $\text{R}_2\text{Fe}_{14}\text{B}$ and R_2Co_{17} compounds exhibit M_s with relatively low values. In rare-earth intermetallic compounds, the 3d transition metal element substitution can adjust their M_s and magneto-crystalline anisotropy, which has been widely investigated [25, 26]. Therefore, it is interesting to investigate magneto-crystalline anisotropy materials with high saturation magnetisation as MAMs.

In this work, we report the magnetic and microwave absorption properties of $\text{Y}_2\text{Co}_{17-x}\text{Fe}_x$ ($x = 0, 5, 9, 13, 17$). The properties of $\text{Y}_2\text{Co}_{17-x}\text{Fe}_x$ compounds can be modified using the 3d transition metal Fe element substitution for Co, which affects the saturation magnetisation, magneto-crystalline anisotropy, and microwave absorption properties. The influence of different magneto-crystalline anisotropy on the microwave absorption properties of the composites is discussed. It is found that the Fe substitution for Co improves successively the microwave absorption performance, as the magneto-crystalline anisotropy changes from axis to plane and then to cone. The $\text{Y}_2\text{Co}_8\text{Fe}_9$ /paraffin composite, with conical

anisotropy and higher M_s , exhibits the most excellent microwave absorption performance.

2 Materials and methods

2.1 Preparation

$Y_2Co_{17-x}Fe_x$ ($x = 0, 5, 9, 13, 17$) alloys were synthesised using high-purity elements by induction melting in an argon atmosphere. An additional 5 wt.% Y was added to compensate for the expected losses from melt evaporation of Y. The alloys were mechanically ground into a powdered form and sifted through a 200-mesh sieve. To attain a uniform microstructure of the powders, it was milled using a high-energy planetary ball mill (XQM-4, Changsha Tencan Powder Technology Co., Ltd.) for 2 h at a rotation rate of 300 rpm under inert conditions with absolute ethanol (99.7%, Sinopharm Group Chemical Reagent Co., Ltd.) as the milling medium. The ball-to-powder weight ratio was 40:1. The milled powders were dried in a vacuum drying chamber at 60 °C for 12 h. To investigate the microwave absorption properties of the compounds, the powders were mixed with paraffin in a 3:2 mass ratio and dispersed in n-hexane in an ultrasonic bath. Then, the composites were dried in a fume hood for 12 h. The $Y_2Co_{17-x}Fe_x$ /paraffin ($x = 0, 5, 9, 13, 17$) composites were compressed into toroidal cores (outer diameter = 7.00 mm, inner diameter = 3.04 mm) using a hydraulic press at a pressure of 2 MPa. To analyse the magneto-crystalline anisotropy of the $Y_2Co_{17-x}Fe_x$ /paraffin composites, the composites were oriented under a rotated magnetic field of 1.7 T.

2.2 Characterisation

The morphological analysis of the $Y_2Co_{17-x}Fe_x$ ($x = 0, 5, 9, 13, 17$) powders was carried out by scanning electron microscopy (SEM; ZEISS EVO18). Particle size distribution was evaluated using a laser particle size analyser (LPSA, HELOS-OASIS). The magnetic properties of the powders were measured by a vibrating sample magnetometer (VSM, Lakeshore7410) at room temperature. The crystal structures and magnetic oriented $Y_2Co_{17-x}Fe_x$ composites were characterised through X-ray diffraction analysis using X-ray diffraction (XRD, Bruker D8 ADVANCE) with a Cu-K α radiation source. The complex

permittivity and permeability of the composites were measured using coaxial method [27, 28] by vector network analyser (VNA, Agilent N5225A) in the range from 1 to 18 GHz.

3 Results and discussion

3.1 Crystalline phase and microstructure

Figure 1a indicates that the $Y_2Co_{17-x}Fe_x$ ($x = 0, 5, 9, 13, 17$) composites exhibit the rhombohedral Th_2Zn_{17} -type structure [20]. The diffraction peaks of the composites shift to the lower angles with the increase of Fe content since the Fe atom is larger than the Co atom. Figure 1b shows the XRD patterns of the magnetically aligned $Y_2Co_{17-x}Fe_x$ composites. The (006) crystal plane increases dramatically whereas other peaks decrease or even disappear, indicating that the easy magnetisation direction (EMD) is in the (006) plane for the $x = 0, 13$, and 17 composites. Thus, these composites have planar anisotropy. For the $x = 5$ composite, the strong diffraction peaks are (300) and (220), indicating that its EMD is parallel to the c-axis and the composite has uniaxial anisotropy. Furthermore, the oriented $x = 9$ composite has a strong peak corresponding to (220) and (006) reflections, suggesting that the composite has conical anisotropy with its EMD lying between the c-axis and the (006) plane. The transition between uniaxial and planar anisotropy may result in a conical anisotropy, which is consistent with the results reported in previous studies [29, 30]. Figure 1c shows the magneto-crystalline anisotropy of $Y_2Co_{17-x}Fe_x$ with increasing Fe content. The EMD changes from plane to axis, then to cone, and eventually to plane. In the rhombohedral Th_2Zn_{17} -type structure, the anisotropy is caused by the interaction between crystal electric field and ion orbit magnetic moment [30]: with a small amount of Fe substituted for Co in the dumbbell 6c sites, the negative contribution (basal plane) will be reduced, leading to a change in the magneto-crystalline anisotropy from plane to axis. When the Fe content increases such that Fe occupies the 18f site, the positive contribution (c-axis) will be reduced and the magneto-crystalline anisotropy turns to the plane.

Figure 2a–j shows the SEM images of the raw and milled $Y_2Co_{17-x}Fe_x$ ($x = 0, 5, 9, 13, 17$) powders. Figure 2k–o presents the particle size distributions of

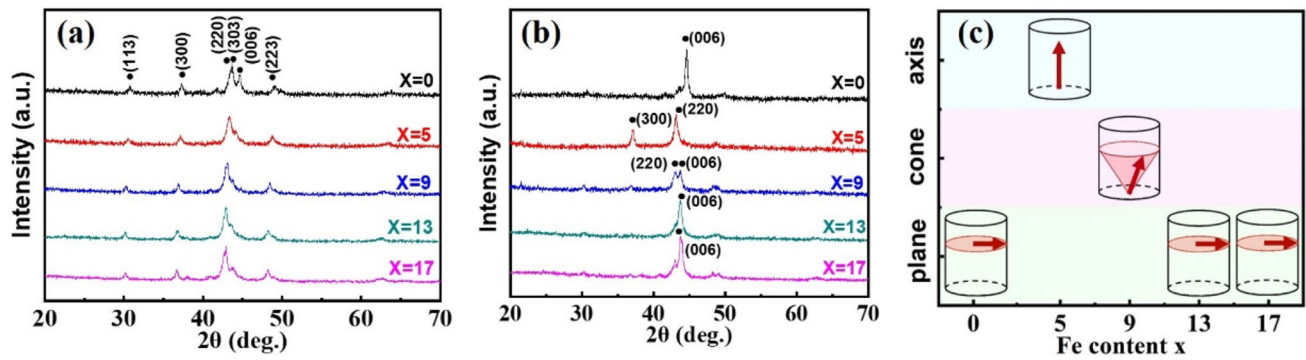


Fig. 1 XRD pattern of **a** randomly and **b** magnetically oriented $Y_2Co_{17-x}Fe_x$ /paraffin ($x = 0, 5, 9, 13, 17$) composites; **c** easy magnetisation direction of $Y_2Co_{17-x}Fe_x$ composites with increasing Fe content

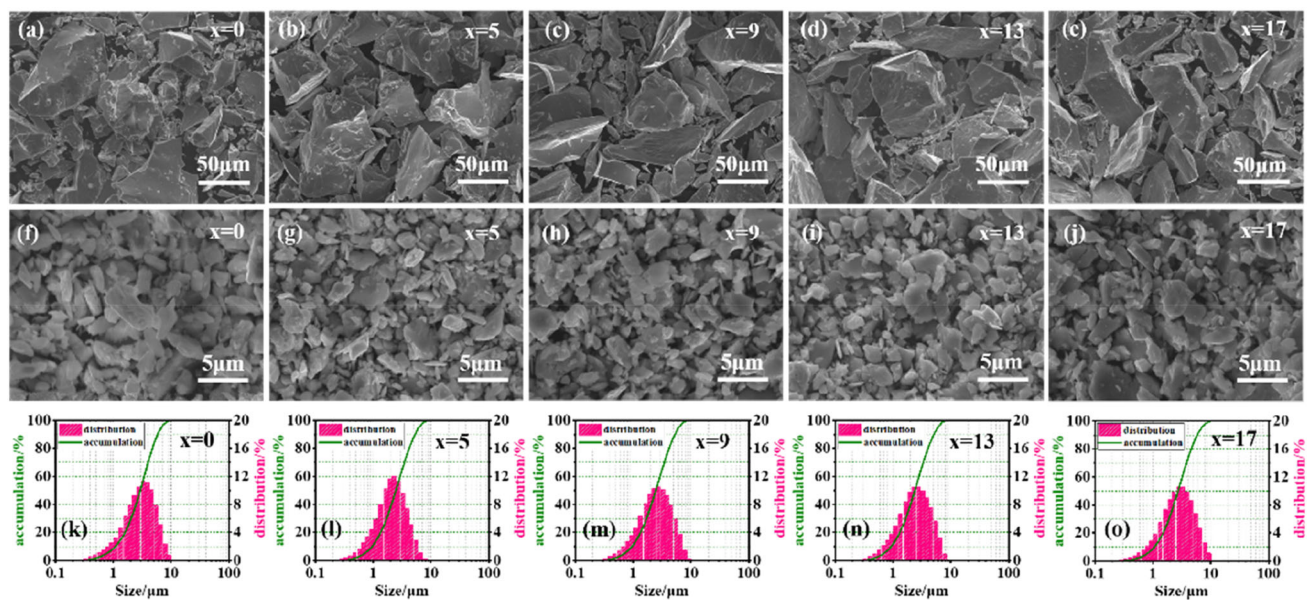


Fig. 2 SEM images of **a–e** raw and **f–j** milled $Y_2Co_{17-x}Fe_x$ ($x = 0, 5, 9, 13, 17$) powders and **k–o** particle size distributions of the milled $Y_2Co_{17-x}Fe_x$ powders ($x = 0, 5, 9, 13, 17$)

powders after ball milling. From Fig. 2, after high-energy planetary ball milling, the morphology transforms from large particles with an average diameter of $40\ \mu\text{m}$ gradually to small particles with an approximate length of $3\text{--}7\ \mu\text{m}$ and thickness of $0.2\text{--}1\ \mu\text{m}$. Because of the large compression and shear forces acting on the particles during ball milling, these particles undergo plastic deformation and welding effect together. The plastic deformation results in the formation of small flaky particles, whilst the welding effect causes a small part of the particles to fuse to each other and form multi-layered flakes. Generally, the skin depth (penetration depth) for metals is approximately $1.3\text{--}3.2\ \mu\text{m}$ at $2.45\ \text{GHz}$ [31]. After the high-energy ball milling, the thickness of

most of the particles is less than the skin depth, which is beneficial to reduce the eddy current and improve microwave absorption performance.

3.2 Static magnetic properties

Figure 3a shows the hysteresis loops for the compounds of $Y_2Co_{17-x}Fe_x$ ($x = 0, 5, 9, 13, 17$) under an applied magnetic field of $\pm 10\ \text{kOe}$ at room temperature. The inset in this figure is an enlarged view of the hysteresis loops. The values of saturation magnetisation (M_s) and coercivity (H_c) are summarised in Fig. 3b. As the Fe content increases, the M_s value is initially $121.22\ \text{emu/g}$ for $x = 0$, increases to 133.72

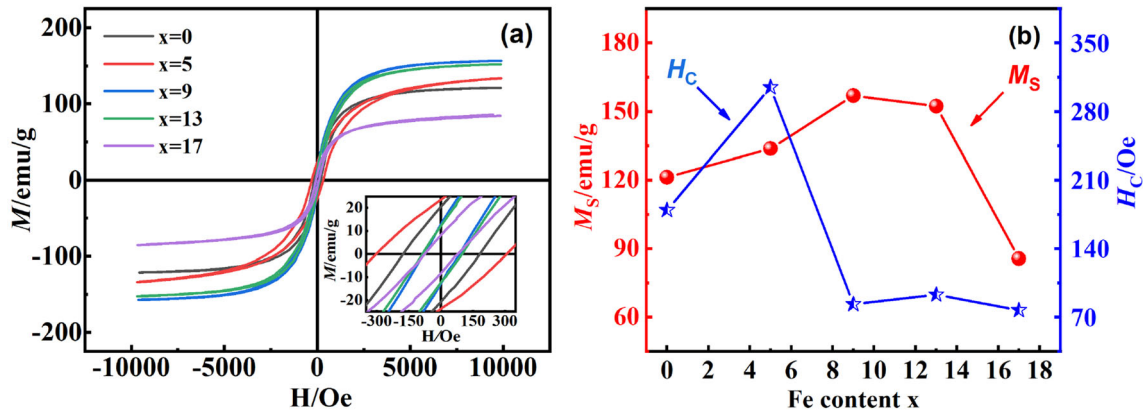


Fig. 3 **a** Hysteresis loops of $Y_2Co_{17-x}Fe_x$ ($x = 0, 5, 9, 13, 17$) compounds at room temperature. **b** The extracted M_s and H_c from the hysteresis loops

emu/g for $x = 5$, and reaches a maximum of 156.89 emu/g at $x = 9$. With a further increase in the Fe content, M_s decreases successively to 152.34 emu/g for $x = 13$ and 85.53 emu/g for $x = 17$. Thus, the M_s values of the $Y_2Co_{17-x}Fe_x$ composites increase first and then decrease with increasing Fe content. These results can be explained in terms of the band model [26]: with the substitution of Fe for Co, the down spin band starts to empty first, enhancing the net magnetic moment; when the M_s value reaches maximum, the d band is entirely occupied by the up spin band such that finally, the up spin band begins to decrease, reducing the net magnetic moment. Furthermore, as Fe substitution increases, the H_c values increase significantly, reach a maximum at $x=5$, and then decrease, which is mainly attributed to the change in magnetic anisotropy [32, 33].

3.3 Microwave absorbing properties

It is well known that the interaction between materials and electromagnetic waves is characterised by complex permeability ($\mu_r = \mu' - j\mu''$) and complex permittivity ($\epsilon_r = \epsilon' - j\epsilon''$) [34]. The real parts of the complex permeability (μ') and permittivity (ϵ') represent the storage abilities of the magnetic and electrical energies, whilst the imaginary parts (μ'' , ϵ'') represent the dissipation abilities [35]. Figure 4a and b presents the frequency dependence of the complex permeability of $Y_2Co_{17-x}Fe_x$ /paraffin composites. The permeability and natural resonance frequency are significantly different for composites with different Fe contents. As shown in Fig. 4a, the values of the

real part of permeability (μ') for the $x = 0, 5, 9, 13$, and 17 composites are 1.61, 1.40, 1.95, 1.76, and 1.55 at 1 GHz, respectively. As the frequency increases, the μ' values of all composites decrease gradually in the 1–18 GHz frequency range. Generally, magnetic loss is mainly attributed to hysteresis, domain wall resonance, natural resonance, and eddy currents [15]. The magnetic loss caused by hysteresis is negligible in a weak applied field, and the domain wall resonance usually occurs in the MHz range. The contribution of eddy currents could be also deemed negligible due to the small particle size and the insulator matrix of the composites. Therefore, the natural resonance is the main factor influencing the magnetic loss in this study. As shown in Fig. 4b, the $x = 0, 9, 13$, and 17 composites have a broad peak (natural resonance peak) in the imaginary part of the complex permeability at approximately 10 GHz. The resonance peak is attributed to the magneto-crystalline anisotropy. However, the $x = 5$ composite has a gradually decreasing μ'' value and its natural resonance peak may be in the MHz range. Compared to the uniaxial anisotropy material, the planar anisotropy material can augment the Snoek limit, which means its high permeability and high resonance frequency can be obtained simultaneously. As a result, the $x = 0, 9, 13$, and 17 composites with the planar (conical) anisotropy have a higher natural resonance frequency than the $x = 5$ composite with uniaxial anisotropy. It can be also observed that both the real and imaginary parts of permeability of the composites with planar (conical) anisotropy are higher than that the composite with uniaxial anisotropy composites. In planar anisotropy composites, the composites with high M_s

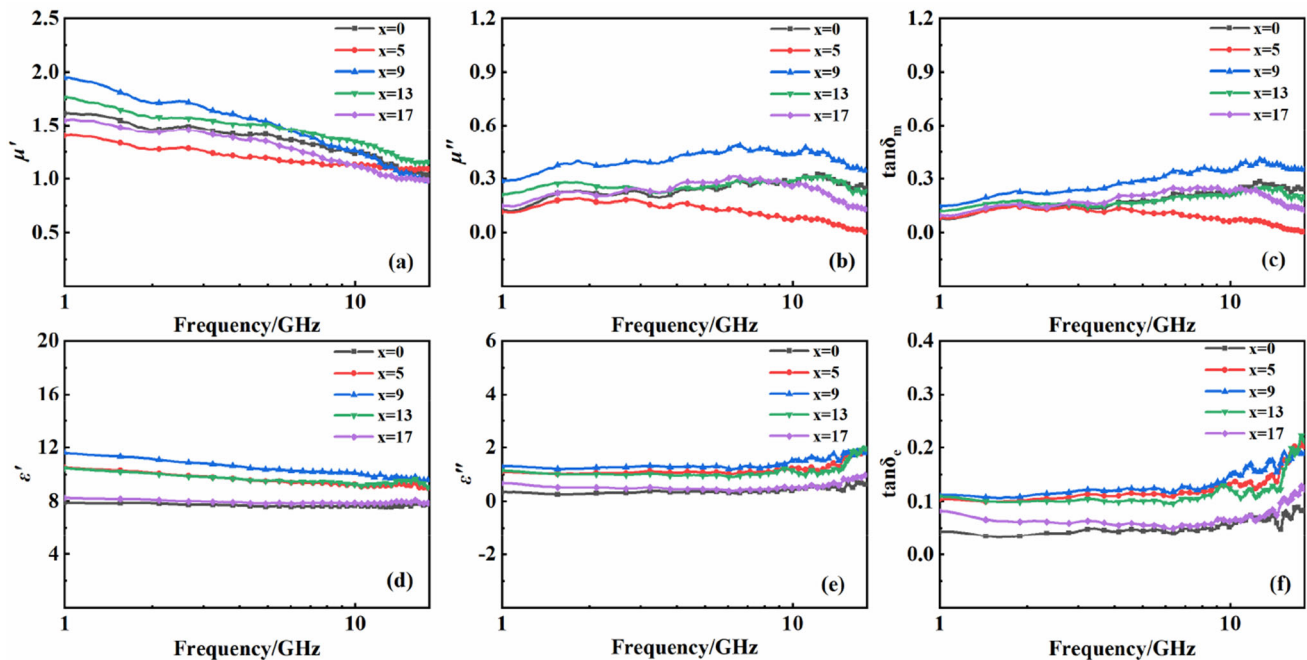


Fig. 4 a, b Complex permeability, c magnetic loss tangent, d, e complex permittivity, and f dielectric loss tangent spectra of $Y_2Co_{17-x}Fe_x$ /paraffin composites ($x = 0, 5, 9, 13, 17$)

tend to have high permeability. The permeability of $x = 9$ composite with conical anisotropy reaches a maximum value.

For magnetic microwave absorbents, high permeability and appropriate permittivity values are performance indicators for strong microwave absorption. Figure 4d and e displays the frequency dependence of the real part of the complex permittivity (ϵ') and the imaginary part (ϵ'') of the composites, respectively. The complex permittivity of $Y_2Co_{17-x}Fe_x$ /paraffin composites is practically independent of the frequency and only fluctuates slightly between 10 and 18 GHz. The ϵ' values of the composites at 1 GHz for $x = 0, 5, 9, 13$, and 17 are 7.87, 10.48, 11.56, 10.43, and 8.24, respectively. The ϵ'' values of the composites at 1 GHz for $x = 0, 5, 9, 13$, and 17 are 0.27, 1.09, 1.29, 0.67, and 1.65, respectively. The permittivity values of composites increase first and then decrease with the increase of Fe content. The calculated magnetic ($\tan\delta_m = \mu''/\mu'$) and dielectric loss tangents ($\tan\delta_e = \epsilon''/\epsilon'$) of all the composites are shown in Fig. 4c and f, which determine the ability to attenuate the electromagnetic waves. The magnetic loss tangent and dielectric loss tangent exhibit trends significantly similar to those of μ'' and ϵ'' , respectively. A low magnetic loss tangent is found for the

$x = 5$ composite, whilst low dielectric loss tangents are found for the $x = 0$ and $x = 17$ composites, which cause a reduction in their absorption effectiveness. In addition, compared to the other composites, the $x = 9$ composite has the highest dielectric loss tangent and magnetic loss tangent, which suggests that this composite would absorb electromagnetic waves most effectively.

Based on the transmission line theory, the electromagnetic reflection loss (RL) can be calculated using parameters for the complex permeability and permittivity as shown in the following Eqs. [36, 37]:

$$RL = 20 \lg |(Z_{in} - Z_0)/(Z_{in} + Z_0)| \quad (3)$$

$$Z_{in} = Z_0 \sqrt{\mu_r/\epsilon_r} \tanh(j(2\pi fd/c)\sqrt{\mu_r\epsilon_r}) \quad (4)$$

where Z_{in} and Z_0 represent the impedances of the absorbent and free space, respectively; d is the thickness of the absorbent; f is the frequency of the electromagnetic wave; and c is the propagation velocity of light. Generally, when the RL value of the absorbent is less than -10 dB, 90% of the incident electromagnetic waves can be consumed by the absorbent, at which point it becomes useful for practical applications [38]. To investigate the microwave absorption properties of the $Y_2Co_{17-x}Fe_x$ /paraffin composites, the RL values of composites with thicknesses from 1 mm to 3 mm are calculated

as shown in Fig. 5. For $x = 0$, with d values of 1.4, 1.8, 2.2, and 2.6 mm, the minimum RLs are obtained -13.1 , -13.8 , -11.8 , and -10.3 dB at 18, 14, 11.1, and 9.4 GHz, respectively. The minimum RLs of the $x = 13$ composite with d values of 1.4, 1.8, 2.2, and 2.6 mm reach -23.2 , -15.6 , -14 , and -12.8 dB at 16.3, 12, 9.7, and 8.1 GHz, respectively. Similarly, for the $x = 17$ composite, the minimum RLs are -11.1 , -11.8 , -12.7 , and -11.8 dB at 17.9, 15, 11.7, and 9.2 GHz when the d value is 1.4, 1.8, 2.2, 2.6mm, respectively. However, the minimum RL of -10 dB could not be reached for the $x = 5$ composite, which implies that its electromagnetic wave absorption is inadequate. Furthermore, the $x=9$ composite exhibits significantly stronger microwave absorption capacity, with minimum RL values below -20 dB at 1.4, 1.8, 2.2, and 2.6mm. The minimum RL values of the $Y_2Co_8Fe_9$ /paraffin composite are -21.4 , -28.2 , -37.8 , and -27.7 dB at 16.2, 11.8, 9.2, and 7.6 GHz at 1.4, 1.8, 2.2, and 2.6mm in sequence.

To further elucidate the microwave absorption characteristics of the investigated $Y_2Co_{17-x}Fe_x$ /paraffin composites, the detailed RL and absorption bandwidth are displayed in Fig. 6. And the influence that the magneto-crystalline anisotropy has on the microwave absorption properties are discussed. For the $x = 5$ composite with uniaxial anisotropy, the

minimum RL values do not reach -10 dB and the effective absorption bandwidth (EAB) is zero. For the $x = 0, 13$, and 17 composites with planar anisotropy, RL values (< -10 dB) are obtained at various thicknesses, with the largest EAB found at approximately 4.05 GHz at 1.7 mm ($x = 0$), 5.31 GHz at 1.5 mm ($x = 13$), and 2.6 GHz at 2.1 mm ($x = 17$). The minimum RL values of the $x=9$ composite with conical anisotropy reach below -10 dB with a relatively wide thickness of 1.2 mm–3 mm. Furthermore, its EAB reaches 6.8 GHz at 1.6 mm. In most practical cases, it is widely accepted that an RL value of less than -20 dB is evidence of a high absorption effectiveness and indicates that 99% of the incident electromagnetic waves can be absorbed [39, 40]. The $x = 9$ composite reaches RLs below -20 dB at 1.3–3 mm and the largest absorption bandwidth (< -20 dB) reaches 1.54 GHz at 1.8 mm. The $x = 9$ composite with conical anisotropy has the highest absorption effectiveness of all the composites investigated. As can be seen in Figs. 5 and 6, the $Y_2Co_8Fe_9$ /paraffin composite exhibits the highest microwave absorption with a minimum RL value of 46.9 dB and an absorption bandwidth of 4.74 GHz with a thickness of 2 mm at a frequency of 10.2 GHz. Except for $x = 5$, the $Y_2Co_{17-x}Fe_x$ /paraffin composites demonstrate significant microwave absorption effectiveness, which is attributed to the anisotropy: composites ($x = 0, 9, 13$,

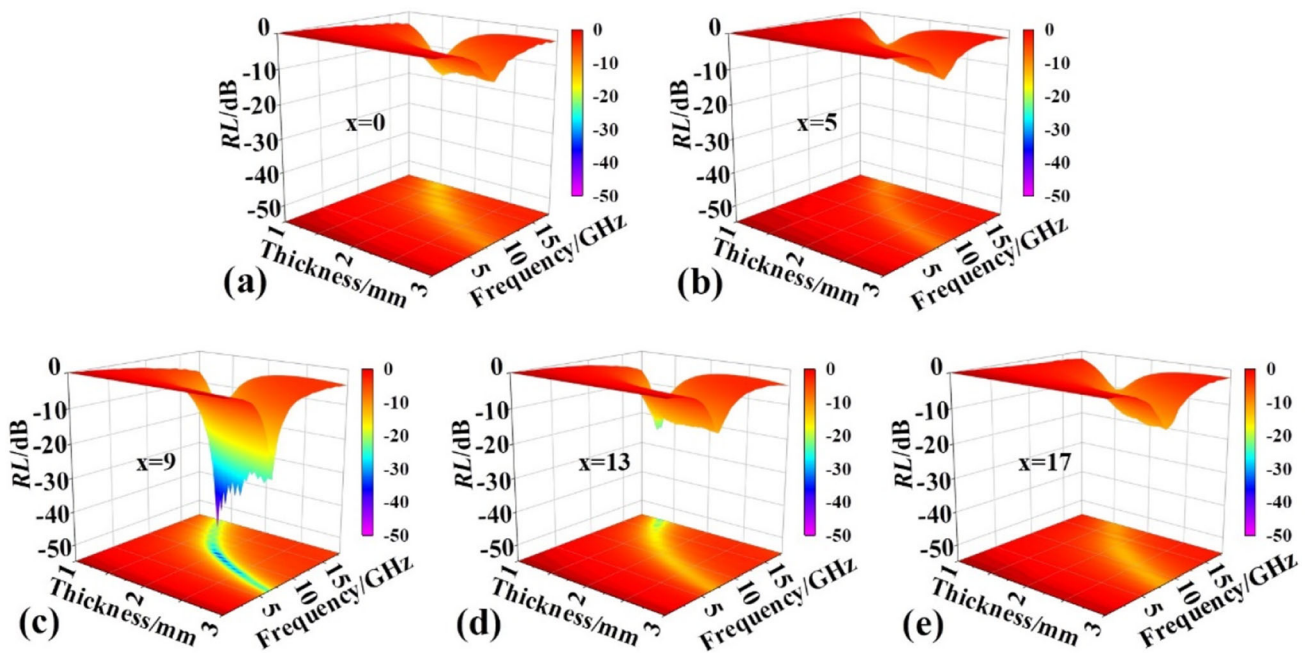


Fig. 5 a–e 3D RL plots of the $Y_2Co_{17-x}Fe_x$ /paraffin composites ($x = 0, 5, 9, 13, 17$) with various thicknesses versus frequency

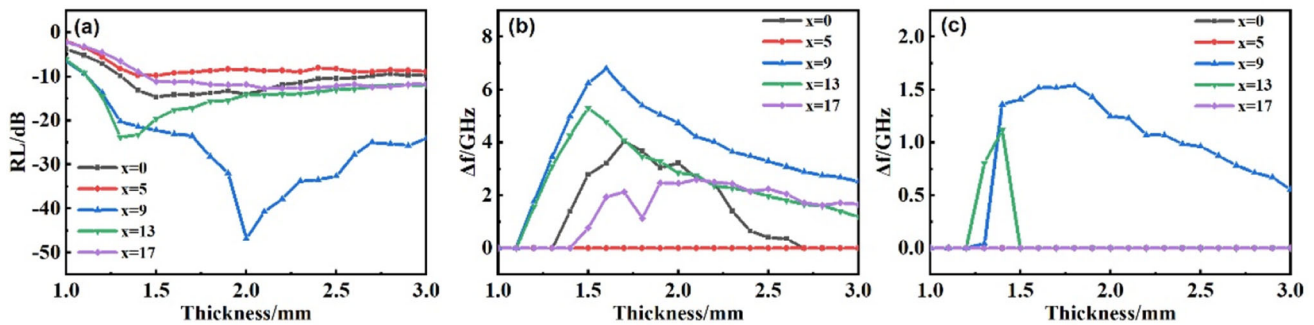


Fig. 6 **a** The minimum RL, **b** effective absorption bandwidth (EAB, RL < -10 dB), and **c** absorption bandwidth (RL < -20 dB) with different thicknesses

17) with planar (conical) anisotropy exhibit higher permeability and resonance peak frequency than the ($x = 5$) composite with uniaxial anisotropy. The high gigahertz frequency permeability could be benefit to optimise the impedance matching and stronger attenuation, enhancing the microwave absorption effectiveness.

It has been reported that high-performance MAMs should satisfy two conditions: optimised impedance matching between free space and MAMs and a strong intrinsic attenuation characteristic of the corresponding electromagnetic waves [41]. The first condition ensures the maximum possible penetration of electromagnetic waves into the interior of the MAMs and the second condition represents the ability with which the incident electromagnetic waves are absorbed. Thus, the attenuation constant (α) [42, 43] and the relative input impedance (Z) [44] of the $Y_2Co_{17-x}Fe_x$ /paraffin composites are calculated for further discussion, using the following equations:

$$Z = |Z_{in}/Z_0| = \sqrt{\mu_r/\epsilon_r} \tanh\left(j\left(\frac{2\pi fd}{c}\right)\sqrt{\mu_r\epsilon_r}\right) \quad (5)$$

$$\alpha = \frac{\sqrt{2}\pi f}{c} \times \sqrt{(\mu''\epsilon'' - \mu'\epsilon') + \sqrt{(\mu''\epsilon'' - \mu'\epsilon')^2 + (\mu''\epsilon' - \mu'\epsilon'')^2}} \quad (6)$$

As mentioned above, the input impedance (Z_{in}) is a key parameter in determining the properties of MAMs and should be matched with the free space impedance (Z_0). According to the rules of impedance matching, the closer the value of relative input

impedance (Z_{in}/Z_0) is to 1, the better is the impedance matching [39].

Figure 7a shows the relative input impedance (Z_{in}/Z_0) of the $Y_2Co_{17-x}Fe_x$ /paraffin composites. It can be seen that the impedance matching of the composites optimises as the magneto-crystalline anisotropy changes from axis to plane and then to cone. To effectively absorb electromagnetic waves, the relative input impedance value should be close to 1 [39]. The $x = 9$ composite with conical anisotropy exhibits comparatively better impedance matching, whilst the other composites exhibit relative input impedance values larger than 1 in the frequency range of 2–18 GHz. The $x = 5$ composite with uniaxial anisotropy exhibits the poorest impedance matching. As can be seen in Fig. 7b, the values of α increase notably with increasing frequency, indicating the enhanced microwave attenuation ability at higher frequencies for the composites. It can also be seen that the values of α increase as the magneto-crystalline anisotropy of the composites changes from axis to plane and then to cone, revealing the gradual increase in microwave attenuation capacity. Based on the microwave absorption properties of all investigated composites, the $Y_2Co_8Fe_9$ /paraffin composite exhibits the optimal impedance matching and strongest microwave attenuation capacity, which is consistent with the RL values shown in Figs. 5 and 6.

As can be seen in Fig. 5, the minimum RL values of the composites shift to the low-frequency location with the increase of the absorbent thickness. To better understand the mechanism, the quarter-wavelength cancellation model is applied to account for the microwave absorption of the absorbent, which can be described as follows [45, 46]:

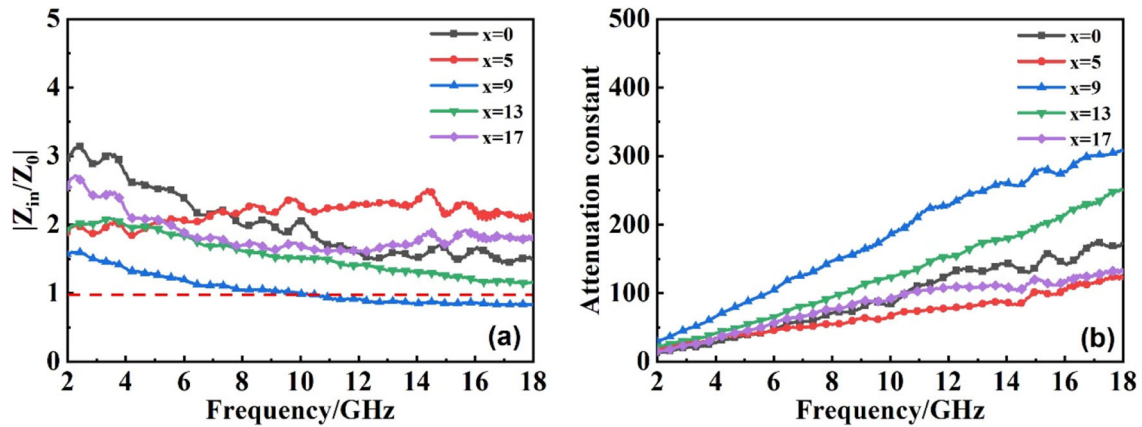


Fig. 7 a Relative input impedance and b attenuation constant of the $Y_2Co_{17-x}Fe_x$ /paraffin composites

$$t_m = \frac{nc}{4f_m \sqrt{|\epsilon_r| |\mu_r|}}, n = 1, 3, 5, \dots \quad (7)$$

where t_m , c , and f_m are the matching thickness, light velocity, and absorption peak frequency, respectively. Electromagnetic waves in the absorbent is partially absorbed, and the rest of the electromagnetic waves is reflected to the free space by the absorbent-metal interface and causes interference with the electromagnetic waves reflected by the air-absorbent interface. When the thickness satisfies Eq. 7, the phase difference between the two electromagnetic

waves is 180° , resulting in destructive interference at the air-absorbent interface [41]. Figure 8 displays the relationship between the minimum RL, matching thickness (t_m), and relative input impedance of the $Y_2Co_8Fe_9$ /paraffin composite at a given frequency. The red five-point stars on the $1/4\lambda$ curves are the matching thickness, and the corresponding frequencies are obtained from the absorption peaks of the RL curves. It can be clearly observed that the thicknesses values in relation to the peaks of the RL curves coincide with the t_m , which suggests that the location of the minimum RL values can be explained by the quarter-wavelength cancellation model. Furthermore, the peaks of the minimum RL is elucidated by the quarter-wavelength cancellation model and the optimal impedance matching.

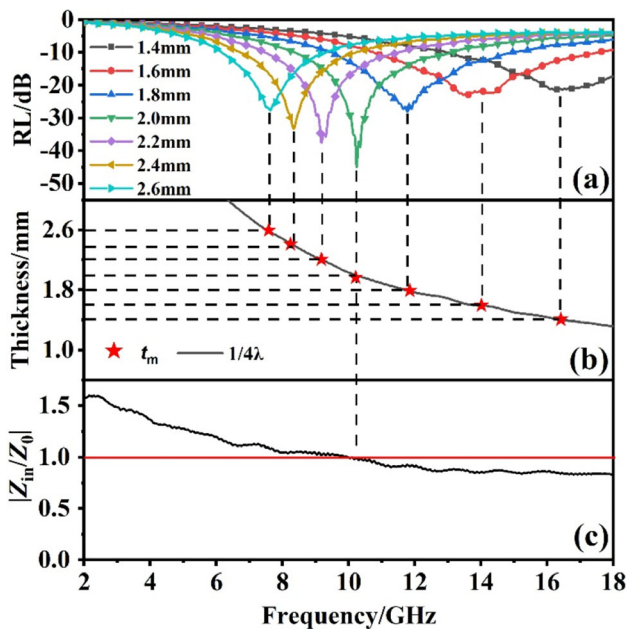


Fig. 8 Frequency-dependent a RL values at different thicknesses, b $\lambda/4$ thickness; c relative input impedance of the $Y_2Co_8Fe_9$ /paraffin composites

A comparison of comprehensive microwave absorption properties of some representative composites is summarised in the GHz range in Table 1. The comprehensive properties mainly include filling ratio, optimal RL, EAB, and their corresponding thickness. Compared with other composites, the $Y_2Co_8Fe_9$ /paraffin composite exhibits excellent microwave absorption property in the GHz range, confirming that it has better comprehensive application performance at high frequency.

4 Conclusion

In summary, our study clearly demonstrates the design of an excellent electromagnetic wave absorbent by adjusting the magneto-crystalline anisotropy.

Table 1 Comparison of microwave absorption properties of some representative composites

Composites	Filling ratio	Optimal RL (dB)	Thickness (mm)	EAB (GHz)(RL < - 10 dB)	References
Ce _{1.7} MM _{0.3} Co _{1.7} /wax	80wt.%	- 40.17	1.8	3.2 (7.44–10.64)	[24]
Ni/SiC/epoxy	80wt.%	- 31.04	3.5	3.44 (6.68–10.12)	[47]
MoS ₂ /epoxy	60wt.%	- 38.4	2.4	4.1 (9.6–13.7)	[48]
SrFe ₁₁ Zn _{0.5} Ni _{0.5} O ₁₉ /epoxy	80wt.%	- 29.62	2.5	3.7 (8.28–11.98)	[49]
FeNi/paraffin	80wt.%	- 37.9	4.0	0.51 (2.19–2.70)	[50]
SnO ₂ /Fe ₃ O ₄ /MWCNTs/ paraffin	70wt.%	- 42	1.9	2.8 (9.6–12.4)	[51]
Y ₂ Co ₈ Fe ₉ /paraffin	60wt.%	- 46.9	2	4.74 (8.38–13.12)	This work

The magneto-crystalline anisotropy of the Y₂Co_{17-x}Fe_x composites change from plane to axis, then to cone, and eventually to plane with increasing Fe substitution. The optimum permeability and resonance frequency, as well as improved microwave absorption properties are achieved in conical anisotropy composites. The Y₂Co₈Fe₉ composite with conical anisotropy and high saturation magnetisation exhibits the best electromagnetic wave absorption capacity of all the composites investigated and is therefore a potential MAM for high-frequency microwave absorption applications.

Acknowledgements

This research was funded by Ningbo Key Project of Scientific and Technical Innovation 2025 (Grant No. 2018B10085 and 2018B10031), Zhejiang Provincial Key Research and Development Projects (Grant No. 2021C01033), the Science and Technology Service Network Initiative regional Key Project of The Chinese Academy of Sciences (Grant No. KFJ-STS-QYZD-2021-07-002), and K. C. Wong Magna Fund in Ningbo University.

References

- A. Yilmaz, L. Tumkaya, K. Akyildiz et al., *J. Maternal-Fetal Neonatal Med.* **30**, 1355 (2017). <https://doi.org/10.1080/14767058.2016.1214124>
- S.N. Narayanan, R.S. Kumar, B.K. Potu, S. Nayak, M. Mailankot, *Clinics* **64**, 231 (2009). <https://doi.org/10.1590/s1807-59322009000300014>
- Y. Bhattacharjee, D. Chatterjee, S. Bose, *ACS Appl. Mater. Interfaces* **10**, 30762 (2018). <https://doi.org/10.1021/acsami.8b10819>
- L. Long, W. Zhou, P. Xiao, Y. Li, *J. Mater. Sci. Mater. Electron.* **30**, 3359 (2019). <https://doi.org/10.1007/s10854-018-00609-x>
- X. Guo, Z. Yao, H. Lin et al., *J. Magn. Magn. Mater.* **485**, 244 (2019). <https://doi.org/10.1016/j.jmmm.2019.04.059>
- Y. Yao, C. Zhang, Y. Fan, J. Zhan, *Adv. Powder Technol.* **27**, 2285 (2016). <https://doi.org/10.1016/j.apt.2016.08.022>
- M.S. Cao, J. Yang, W.L. Song et al., *ACS Appl. Mater. Interfaces* **4**, 6949 (2012). <https://doi.org/10.1021/am3021069>
- K. Manna, S.K. Srivastava, *ACS Sustain. Chem. Eng.* **5**, 10710 (2017). <https://doi.org/10.1021/acssuschemeng.7b02682>
- X. Huang, J. Zhang, Z. Liu et al., *J. Alloys Compd.* **648**, 1072 (2015). <https://doi.org/10.1016/j.jallcom.2015.07.073>
- Y. Yuan, S. Wei, Y. Liang, B. Wang, Y. Wang, *Materials* (2020). <https://doi.org/10.3390/ma13235331>
- Y. Zhao, L. Liu, J. Han, W. Wu, G. Tong, *J. Alloys Compd.* **728**, 100 (2017). <https://doi.org/10.1016/j.jallcom.2017.08.238>
- G. Qiao, Q. Hu, P. Zhang et al., *J. Alloys Compd.* **825**, 154179 (2020). <https://doi.org/10.1016/j.jallcom.2020.154179>
- D. He, Z. Dou, J. Zhang et al., *J. Magn. Magn. Mater.* **513**, 167191 (2020). <https://doi.org/10.1016/j.jmmm.2020.167191>
- W. Yang, Y. Zhang, G. Qiao et al., *Acta Mater.* **145**, 331 (2018). <https://doi.org/10.1016/j.actamat.2017.12.042>
- G. Tan, Y. Zhang, L. Qiao, T. Wang, J. Wang, F. Li, *Phys. B* **477**, 52 (2015). <https://doi.org/10.1016/j.physb.2015.08.012>
- L.Z. Li, J.Z. Wei, Y.H. Xia et al., *Appl. Phys. Lett.* (2014). <https://doi.org/10.1063/1.4889806>
- J. Yang, W. Yang, F. Li, Y. Yang, *J. Magn. Magn. Mater.* (2019). <https://doi.org/10.1016/j.jmmm.2019.165961>
- T. Wang, C. Pan, Y. Wang et al., *J. Magn. Magn. Mater.* **354**, 12 (2014). <https://doi.org/10.1016/j.jmmm.2013.10.045>

19. Z.W. Li, Y.P. Wu, G.Q. Lin, L. Chen, J. Magn. Magn. Mater. **310**, 145 (2007). <https://doi.org/10.1016/j.jmmm.2006.08.003>
20. X. Gu, G. Tan, S. Chen et al., J. Magn. Magn. Mater. **424**, 39 (2016). <https://doi.org/10.1016/j.jmmm.2016.10.025>
21. R. Han, H. Yi, J. Wei, L. Qiao, T. Wang, F. Li, Appl. Phys. A **108**, 665 (2012). <https://doi.org/10.1007/s00339-012-6948-9>
22. L.-X. Lian, L.J. Deng, M. Han, W. Tang, S.-D. Feng, J. Appl. Phys. **101**, 207 (2007). <https://doi.org/10.1063/1.2712957>
23. C. He, S. Pan, L. Cheng, X. Liu, Y. Wu, J. Rare Earths **33**, 271 (2015). [https://doi.org/10.1016/s1002-0721\(14\)60414-2](https://doi.org/10.1016/s1002-0721(14)60414-2)
24. S. Yh Liu, L. Pan, J. Cheng, L. Yu, Huang (2020) J. Mater. Sci. Mater. Electron. <https://doi.org/10.1007/s10854-020-03668-1>
25. X. Liu, L. Qiao, F. Li, J. Phys. D: Appl. Phys. (2010). <https://doi.org/10.1088/0022-3727/43/16/165004>
26. Y. Matsuura, S. Hirose, H. Yamamoto, S. Fujimura, M. Sagawa, Appl. Phys. Lett. **46**, 308 (1985). <https://doi.org/10.1063/1.95668>
27. A.M. Nicolson, IEEE Trans. Instrum. Meas. (1970). <https://doi.org/10.1109/TIM.1970.4313932>
28. W.B. Weir, Proc. IEEE (1974). <https://doi.org/10.1109/PROC.1974.9382>
29. X.C. Kou, T.S. Zhao, R. Grossinger, H.R. Kirchmayr, X. Li, F.R. de Boer, Phys. Rev. B Condens. Matter. **47**, 3231 (1993). <https://doi.org/10.1103/physrevb.47.3231>
30. S. Zhang, B. Shen, H. Zhang et al., J. Appl. Phys. **83**, 5326 (1998). <https://doi.org/10.1063/1.367359>
31. J. Sun, W. Wang, Q. Yue, Materials **9**, 231 (2016). <https://doi.org/10.3390/ma9040231>
32. Q. Li, S. Yan, X. Wang et al., Acta Mater. **98**, 190 (2015). <https://doi.org/10.1016/j.actamat.2015.07.038>
33. C. Singh, S.B. Narang, I.S. Hudiara, Y. Bai, K. Marina, Mater. Lett. **63**, 1921 (2009)
34. D. Liu, Y. Zhang, C. Zhou et al., J. Alloys Compd. (2020). <https://doi.org/10.1016/j.jallcom.2019.152861>
35. J. Ouyang, Z. He, Y. Zhang, H. Yang, Q. Zhao, ACS Appl. Mater. Interfaces **11**, 39304 (2019). <https://doi.org/10.1021/acsaami.9b11430>
36. X. Zeng, X. Cheng, R. Yu, G.D. Stucky, Carbon **168**, 606 (2020). <https://doi.org/10.1016/j.carbon.2020.07.028>
37. Y. Wang, W. Zhou, G. Zeng et al., Carbon **175**, 233 (2021). <https://doi.org/10.1016/j.carbon.2021.01.001>
38. H. Liu, Y. Li, M. Yuan et al., ACS Appl. Mater. Interfaces. **10**, 22591 (2018). <https://doi.org/10.1021/acsaami.8b05211>
39. A. Ling, J. Pan, G. Tan et al., J. Alloys Compd. **787**, 1097 (2019). <https://doi.org/10.1016/j.jallcom.2019.02.164>
40. T. Wu, Y. Zhao, Y. Li, W. Wu, G. Tong, ChemCatChem **9**, 3486 (2017). <https://doi.org/10.1002/cctc.201700437>
41. C. Ge, L. Wang, G. Liu, T. Wang, J. Alloys Compd. **767**, 173 (2018). <https://doi.org/10.1016/j.jallcom.2018.07.081>
42. Y. Yuan, S. Wei, Y. Liang et al., J. Magn. Magn. Mater. (2020). <https://doi.org/10.1016/j.jmmm.2020.166791>
43. W. Zhou, Y. Li, L. Long, H. Luo, Y. Wang, J. Am. Ceram. Soc. **103**, 6822 (2020). <https://doi.org/10.1111/jace.17389>
44. F. Chen, H. Luo, Y. Cheng et al., Compos. Part A: Appl. Sci. Manuf. **140**, 106141 (2020)
45. Y. Liu, Y. Lin, H. Yang, J. Alloys Compd. **805**, 130 (2019). <https://doi.org/10.1016/j.jallcom.2019.07.006>
46. Z. Gao, Z. Jia, J. Zhang, A. Feng, Z. Huang, G. Wu, J. Mater. Sci. Mater. Electron. **30**, 13474 (2019). <https://doi.org/10.1007/s10854-019-01715-0>
47. S. Singh, A. Kumar, S. Agarwal, D. Singh, J. Magn. Magn. Mater. **503**, 166616 (2020). <https://doi.org/10.1016/j.jmmm.2020.166616>
48. M.-Q. Ning, M.-M. Lu, J.-B. Li et al., Nanoscale **7**, 15734 (2015). <https://doi.org/10.1039/c5nr04670j>
49. S. Tyagi, H.B. Baskey, R.C. Agarwala, V. Agarwala, TC Shami, Ceram. Int. **37**, 2631 (2011). <https://doi.org/10.1016/j.ceramint.2011.04.012>
50. H. Zhao, Z. Zhu, C. Xiong, X. Zheng, Q. Lin, RSC Adv. **6**, 16413 (2016). <https://doi.org/10.1039/c5ra27179g>
51. L. Wang, H. Xing, Z. Liu, Z. Shen, X. Sun, G. Xu, RSC Adv. **6**, 97142 (2016). <https://doi.org/10.1039/c6ra21092a>

Publisher's Note Springer Nature remains neutral with regard to jurisdictional claims in published maps and institutional affiliations.